

1 The Silicon Vertex Detector of the Belle II Experiment

2 Y. Uematsu^a, K. Adamczyk^t, L. Aggarwal^l, H. Aihara^q, T. Aziz^j, S. Bacher^t,
3 S. Bahinipati^f, G. Batignani^{k,l}, J. Baudot^e, P. K. Behera^g, S. Bettarini^{k,l},
4 T. Bilka^c, A. Bozek^t, F. Buchsteiner^b, G. Casarosa^{k,l}, L. Corona^{k,l}, T. Czank^p,
5 S. B. Das^h, G. Dujany^e, F. Forti^{k,l}, M. Friedl^b, A. Gabrielli^{m,n}, E. Ganiev^{m,n},
6 B. Gobboⁿ, S. Halder^j, K. Hara^{r,o}, S. Hazra^j, T. Higuchi^p, C. Irmiler^b,
7 A. Ishikawa^{r,o}, H. B. Jeon^s, Y. Jin^{m,n}, C. Joo^p, M. Kaleta^t, A. B. Kaliyar^j,
8 J. Kandra^c, K. H. Kang^s, P. Kapusta^t, P. Kodyš^c, T. Kohriki^r, M. Kumar^h,
9 R. Kumarⁱ, C. La Licata^p, K. Lalwani^h, S. C. Lee^s, J. Libby^g, S. N. Mayekar^j,
10 G. B. Mohanty^j, T. Morii^p, K. R. Nakamura^{r,o}, Z. Natkaniec^t, Y. Onuki^q,
11 W. Ostrowicz^t, A. Paladino^{k,l}, E. Paoloni^{k,l}, H. Park^s, G. Polat^d, K. K. Rao^j,
12 I. Ripp-Baudot^e, G. Rizzo^{k,l}, D. Sahoo^j, C. Schwanda^b, J. Serrano^d,
13 J. Suzuki^r, S. Tanaka^{r,o}, H. Tanigawa^q, R. Thalmeier^b, R. Tiwari^j,
14 T. Tsuboyama^{r,o}, O. Verbycka^t, L. Vitale^{m,n}, K. Wan^q, Z. Wang^q, J. Webb^a,
15 J. Wiechczynski^l, H. Yin^b, L. Zani^d,

16 (Belle-II SVD Collaboration)

17 ^a*School of Physics, University of Melbourne, Melbourne, Victoria 3010, Australia*

18 ^b*Institute of High Energy Physics, Austrian Academy of Sciences, 1050 Vienna, Austria*

19 ^c*Faculty of Mathematics and Physics, Charles University, 121 16 Prague, Czech Republic*

20 ^d*Aix Marseille Université, CNRS/IN2P3, CPPM, 13288 Marseille, France*

21 ^e*IPHC, UMR 7178, Université de Strasbourg, CNRS, 67037 Strasbourg, France*

22 ^f*Indian Institute of Technology Bhubaneswar, Satya Nagar, India*

23 ^g*Indian Institute of Technology Madras, Chennai 600036, India*

24 ^h*Malaviya National Institute of Technology Jaipur, Jaipur 302017, India*

25 ⁱ*Punjab Agricultural University, Ludhiana 141004, India*

26 ^j*Tata Institute of Fundamental Research, Mumbai 400005, India*

27 ^k*Dipartimento di Fisica, Università di Pisa, I-56127 Pisa, Italy*

28 ^l*INFN Sezione di Pisa, I-56127 Pisa, Italy*

29 ^m*Dipartimento di Fisica, Università di Trieste, I-34127 Trieste, Italy*

30 ⁿ*INFN Sezione di Trieste, I-34127 Trieste, Italy*

31 ^o*The Graduate University for Advanced Studies (SOKENDAI), Hayama 240-0193, Japan*

32 ^p*Kavli Institute for the Physics and Mathematics of the Universe (WPI), University of
33 Tokyo, Kashiwa 277-8583, Japan*

34 ^q*Department of Physics, University of Tokyo, Tokyo 113-0033, Japan*

35 ^r*High Energy Accelerator Research Organization (KEK), Tsukuba 305-0801, Japan*

36 ^s*Department of Physics, Kyungpook National University, Daegu 41566, Korea*

37 ^t*H. Niewodniczanski Institute of Nuclear Physics, Krakow 31-342, Poland*

38 Abstract

39 The Silicon Vertex Detector (SVD) is a part of the vertex detector in the
40 Belle II experiment at the SuperKEKB collider (KEK, Japan). Since the start
41 of data taking in spring 2019, the SVD has been operating stably and reliably

Email address: uematsu@hep.phys.s.u-tokyo.ac.jp (Y. Uematsu)

Preprint submitted to Nuclear Instruments and Methods A

November 14, 2021

42 with a high signal-to-noise ratio and hit efficiency, achieving good spatial resolu-
43 tion and high track reconstruction efficiency. The hit occupancy, which mostly
44 comes from the beam-related background, is currently about 0.5% in the in-
45 nermost layer, causing no impact on the SVD performance. In anticipation of
46 the operation at higher luminosity in the next years, two strategies to sustain
47 the tracking performance in future high beam background conditions have been
48 developed and tested on data. One is to reduce the number of signal waveform
49 samples to decrease dead time, data size, and occupancy. The other is to utilize
50 the good hit-time resolution to reject the beam background hits. We also mea-
51 sured the radiation effects on the sensor current, strip noise, and full depletion
52 voltage caused during the first two and a half years of operation. The results
53 show no detrimental effect on the SVD performance.

54 *Keywords:* Silicon strip detector, Vertex detector, Tracking detector, Belle II

55 1. Introduction

56 The Belle II experiment [1] aims to probe new physics beyond the Stan-
57 dard Model in high-luminosity e^+e^- collision at the SuperKEKB collider (KEK,
58 Japan) [2]. The SuperKEKB consists of injector LINAC, positron dumping ring,
59 and main storage ring with the electron and positron beamlines. The Belle II
60 detector is located at the interaction point (IP) of the two beamlines. The main
61 collision energy in the center-of-mass system is 10.58 GeV on the $\Upsilon(4S)$ mass-
62 resonance, which enables various physics programs based on the high statistics of
63 B-mesons, τ -leptons, and D-mesons. Also, the asymmetric energy of the 7-GeV
64 electron beam and 4-GeV positron beam is adopted for the time-dependent CP
65 violation measurement. The target of SuperKEKB is to accumulate integrated
66 luminosity of 50 ab^{-1} with peak luminosity of about $6 \times 10^{35} \text{ cm}^{-2}\text{s}^{-1}$. In
67 June 2021, SuperKEKB recorded the world's highest instantaneous luminosity
68 of $3.1 \times 10^{34} \text{ cm}^{-2}\text{s}^{-1}$. The data accumulated before July 2021 is 213 fb^{-1} .

69 The Vertex Detector (VXD) is the innermost detector in the Belle II detector
70 system. The VXD has six layers: the inner two layers (layers-1 and 2) are the

71 Pixel Detector (PXD), and the outer four layers (layers-3 to 6) are the Silicon
 72 Vertex Detector (SVD). The schematic cross-sectional view of the VXD is shown
 73 in Fig. 1. The PXD consists of DEPFET pixel sensors, and its innermost radius
 74 is 1.4 cm from the IP. Detailed descriptions of the SVD appear in Sec. 2.

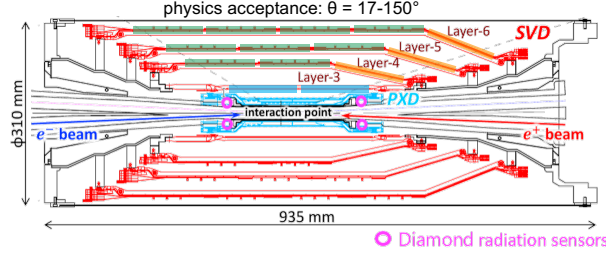


Figure 1: Schematic cross-sectional view of the VXD. The SVD is in red, the PXD in light-blue, and the IP beam pipe diamonds in pink circles. The locations of the three types of DSSDs are indicated by boxes in three colors: blue for small sensors, green for large sensors, and orange for trapezoidal sensors as described in Tab. 1.

75 Besides the VXD, diamond sensors [3] are mounted on the IP beam pipe and
 76 the bellows pipes outside of the VXD. The pink circles in Fig. 1 indicate the
 77 locations of the diamond sensors on the IP beam pipe. They measure the dose
 78 rates in these locations. The measured doses are used to estimate the dose in
 79 the SVD. They also send beam abort requests to SuperKEKB if the radiation
 80 level gets too high to avoid severe damage to the detector.

81 2. Belle II Silicon Vertex Detector

82 The SVD is crucial for extrapolating the tracks to the PXD. This task is
 83 essential for measuring the decay vertices with the PXD and pointing at a region-
 84 of-interest limiting the PXD readout volume. Also, the SVD plays a critical role
 85 in the decay vertex measurement in case long-lived particles like K_S decay inside
 86 the SVD volume. Other roles of the SVD are the standalone track reconstruction
 87 of low-momentum charged particles and their particle identification using energy
 88 deposit dE/dx .

89 The SVD [4] consists of four layers of Double-sided Silicon Strip Detectors
 90 (DSSDs). The material budget of the SVD is about 0.7% X_0 per layer. The
 91 readout Aluminum strips are AC-coupled to every other n/p-side strips (elec-
 92 trodes) on the n-type substrate over the silicon oxide layer. On each DSSD
 93 plane, a local coordinate is defined with u and v : u -axis along n-side strips and
 94 v -axis perpendicular to u -axis. In other words, p-side strips and n-side strips
 95 provide u and v information, respectively. In the cylindrical coordinate, u cor-
 96 responds to r - φ information and v corresponds to z information. The SVD
 97 consists of three types of sensors: “small” sensors in layer-3, “large” sensors in
 98 layer-456 barrel region, and “trapezoidal” sensors in layer-456 forward/slanted
 99 region. They are indicated in blue, green, and orange boxes in Fig. 1. The
 100 dimensions for these three types of sensors are summarized in Tab. 1. The
 101 sensors are manufactured by two companies: the small and large sensors by
 102 Hamamatsu and trapezoidal sensors by Micron. The full depletion voltage is 60
 103 V for Hamamatsu sensors, 20 V for Micron sensors, and both types of sensors
 104 are operated at 100 V. In total, 172 sensors are assembled, corresponding to a
 105 total sensor area of 1.2 m² and 224,000 readout strips.

	Small	Large	Trapezoidal
No. of u/p-strips	768	768	768
u/p-strip pitch	50 μm	75 μm	50–75 μm
No. of v/n-strips	768	512	512
v/n-strip pitch	160 μm	240 μm	240 μm
Thickness	320 μm	300 μm	300 μm
Manufacturer	Hamamatsu		Micron

Table 1: Table of dimensions for three types of sensors. Only readout strips are taking into account for number of strips and strip pitch.

106 The front-end ASIC used in the SVD is APV25 [5], which was originally
 107 developed for CMS silicon tracker. APV25 is radiation hard for over 100 Mrad
 108 radiation. It has 128 channel inputs and shapers for each channel with a shaping

109 time of about 50 ns. For the SVD, APV25 is operated in “multi-peak” mode.
110 The mechanism of the data sampling in the multi-peak mode is explained in
111 Fig. 2. The chip samples the height of the signal waveform with the 32 MHz
112 clock and stores each sampled information in the analog ring buffer. Since
113 the bunch-crossing frequency is eight times faster than the sampling clock, the
114 stored samples are not synchronous to the beam collision in contrast to CMS,
115 which motivates to operate in the multi-peak mode. In the present readout
116 configuration (the six-samples mode), at every reception of the Belle II global
117 Level-1 trigger, the chip reads out successive six samples of the signal wave-
118 form stored in the buffers. The six-samples mode offers enough time window
119 ($6/32 \text{ MHz}^{-1} = 187 \text{ ns}$) which accepts large timing shifts of the trigger. In
120 preparation for operation with higher luminosity, where background occupancy,
121 trigger dead-time, and the data size increase, we developed the three/six-mixed
122 acquisition mode (mixed-mode). The mixed-mode is a new method to read out
123 the signal samples from APV25, in which the number of the samples changes
124 between three and six in each event, depending on the timing precision of each
125 Level-1 trigger signal in that event. For triggers with good timing precision,
126 three-samples data are read out and the data have half time window and half
127 data size compared to ones of six-samples data, resulting in the reduction of the
128 effect due to higher luminosity. This functionality was already implemented in
129 the running system and confirmed by a few hours of smooth physics data-taking.
130 Before we start to use the mixed-mode, the effect on the performance due to
131 the change of the acquisition mode is to be assessed. As the first step, the effect
132 in the hit efficiency was evaluated as described in Sec. 3.

133 The APV25 chips are mounted on each middle sensor (chip-on-sensor con-
134 cept) with thermal isolation foam in between. The merit of this concept is
135 shorter signal propagation length, leading to the smaller capacitance of the sig-
136 nal line and hence the smaller noise level. To reduce the material budget the
137 APV25 chips on the sensor are thinned down to $100 \mu\text{m}$. APV25s are mounted
138 on the single side of the sensor and read out the signals from the other side via
139 wrapped flexible printed circuits. The power consumption of the APV25 chip

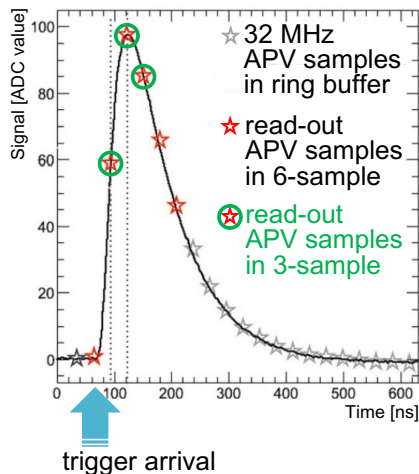


Figure 2: The plot explains the sampling in the “multi-peak” mode of APV25. The black line shows the signal waveform after the CR-RC shaper circuit. The stars show the sampled signal height recorded in the analog ring buffer according to the 32 MHz sampling clock. The red stars indicate the six successive samples read out at the trigger reception in the six-samples mode. The red stars with a green circle indicate the samples read out in the three-samples acquisition.

140 is 0.4 W/chip and in total 700W in the entire SVD. The chips are chilled by
 141 bi-phase -20°C CO_2 .

142 3. Performance

143 The SVD was combined with the PXD to complete the VXD assembly in
 144 October 2018, and the VXD was installed to the Belle II detector system in
 145 November 2018. Since March 2019, the SVD has been operating reliably and
 146 smoothly for two and a half years, without any major problems. The total
 147 fraction of masked strips is about 1%. There was only one issue where one
 148 APV25 chip (out of 1,748 chips) was disabled during the spring of 2019, which
 149 was gone after cable reconnection in the summer of 2019.

150 The SVD has also demonstrated stable and excellent performance [6]. The
 151 hit efficiency is stably over 99% in most of the sensors. The cluster charge dis-

152 tributions are also reasonable. On the u/p-side, the most probable values agree
 153 with the calculated charge amount induced by MIPs within the uncertainty in
 154 calibration. On the v/n-side, 10–30% of the collected charge losses compared to
 155 MIP due to the smaller inter-strip capacitance of the floating strips with larger
 156 strip pitches than the u/p-side. The most probable values of the cluster SNR
 157 distributions range from 13 to 30.

158 We measured the cluster position resolution by analyzing the $e^+e^- \rightarrow \mu^+\mu^-$
 159 data [7]. The cluster position resolution is estimated from the residual between
 160 the cluster position and the track position not biased by the target cluster after
 161 subtracting the effect of the track extrapolation error. The cluster position
 162 resolutions for different incident angles are shown in Fig. 3. For normal incident
 163 tracks, it well agrees with the expectations from the strip pitch including floating
 164 strips. For tracks with an incident angle, it is expected to get a better resolution,
 165 which is indeed the case in the v/n-side results. However, this effect is not
 166 observed on the u/p-side, and the study is still ongoing to improve the cluster
 167 position estimation.

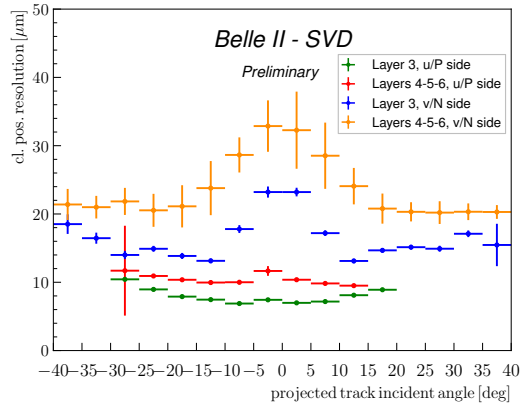


Figure 3: The SVD cluster position resolution depending on the projected track incident angle. The green(blue) plot shows the resolution in the u/p(n/v)-side of Layer 3 sensors, and the red(yellow) one shows the u/p(n/v)-side of Layers 4–6 sensors.

168 The cluster hit-time resolution was also evaluated in the hadron events¹ data
 169 using the reference event time estimated by the Central Drift Chamber (CDC)
 170 outside of SVD. The error on the event time, about 0.7 ns, was subtracted
 171 to evaluate the intrinsic SVD hit-time resolution. The resulting resolution is
 172 2.9 ns on the u/p-side and 2.4 ns on the v/n-side. With such precise hit-
 173 time information, it is possible to reject off-time background hits efficiently.
 174 The hit-time distributions for signal² and off-time background³ are shown in
 175 Fig. 4. The signal distribution has a narrow peak, while the background hit-time
 176 distribution is broad and almost flat in the signal peak region. The separation
 177 power of the hit-time is high, as expected. For example, if we reject hits with
 178 the hit-time less than -38 ns in this plot, we can reject 46% of the background
 179 hits while keeping 99% of the signal hits. The background rejection based on
 180 the hit-time is essential to sustain the good tracking performance in the future
 181 high beam background condition.

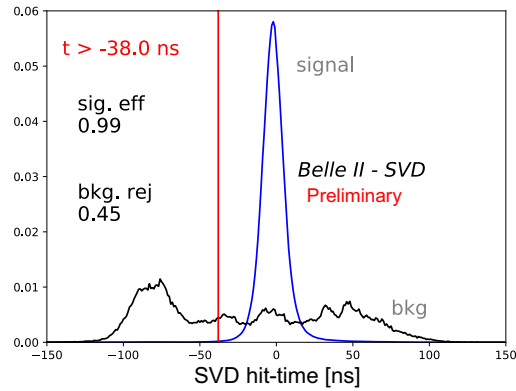


Figure 4: The plot shows an example of the background hit rejection using hit-time. The blue distribution shows the signal, and the black distribution shows the off-time background. Assuming the hit-time cut at -38 ns, the signal hit efficiency of 99% and the background hit rejection of 46% are achieved.

¹The events with more than three good tracks and not like Bhabha scattering.

²The clusters found to be used in the tracks in the hadron events.

³The clusters in events triggered by delayed-Bhabha pseudo-random trigger.

182 The performance in three-samples data was compared with that in six-
 183 samples data to evaluate the performance in the mixed-mode. If the trigger
 184 timing has no deviation, the three-samples data will show comparable perfor-
 185 mance to the six-samples data because the relevant part of the signal waveform
 186 to evaluate the necessary signal properties, which are the signal height and the
 187 signal timing, can be accommodated in the three-samples time window. How-
 188 ever, when the trigger has a jitter and the timing shift happens, some part
 189 of the signal waveform can be out of the three-samples time window, and the
 190 reconstruction performance deteriorates. We examined the effect on the hit ef-
 191 ficiency as a function of the trigger timing shift. The effect is evaluated by the
 192 relative hit efficiency, which is defined as the ratio of the hit efficiency in the
 193 three-samples data to the one in the six-samples data. For this study, the three-
 194 samples data are emulated in the offline analysis from the six-samples data by
 195 selecting consecutive three samples at fixed positions in the six samples. The
 196 trigger timing shift is evaluated by the CDC event time. The resulting relative
 197 efficiencies as a function of the trigger timing shift in the hadron events are
 198 shown in Fig. 5. The decreasing trend is observed for the shift of the trigger
 199 timing, as expected. As a result, the relative efficiency is over 99.9% for the
 200 trigger timing shift within ± 30 ns.

201 **4. Beam-related background effects on SVD**

202 The beam-related background increases the hit occupancy of the SVD, which
 203 in turn degrades the tracking performance. Considering this performance degra-
 204 dation, we set the occupancy limit in layer-3 sensors to be about 3%, which will
 205 be loosened roughly by a factor of two after we apply the hit-time rejection
 206 described in Sec. 3. With the current luminosity, the average hit occupancy in
 207 layer-3 sensors is less than 0.5%. However, the projection of the hit occupancy
 208 at the luminosity of $8 \times 10^{35} \text{ cm}^{-2}\text{s}^{-1}$ is about 3% in layer-3 sensors. The pro-
 209 jected occupancy comes from the Monte Carlo (MC) simulation scaled by the
 210 data/MC ratio determined from the beam background data of the current beam

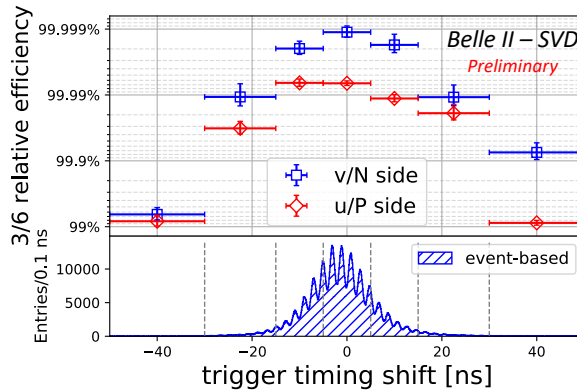


Figure 5: The relative hit efficiencies as a function of the trigger timing shift for v/n-side (blue square) and u/p-side (red diamond). The positive (negative) trigger timing shift corresponds to early (late) trigger timing.

211 optics. The corresponding dose is about 0.2 Mrad/smy, and the equivalent 1-
 212 MeV neutron fluence is about 5×10^{11} $n_{\text{eq}}/\text{cm}^2/\text{smy}$ (smy: Snowmass Year =
 213 10^7 sec). The long-term extrapolation of the beam background is affected by
 214 large uncertainties from the optimization of collimator settings in MC and the
 215 future evolution of the beam injection background, which is not simulated. This
 216 uncertainty motivates the VXD upgrade which improves the tolerance of the hit
 217 rates and the radiation damages, and the technology assessment is ongoing for
 218 multiple sensor options.

219 From the measured dose on diamond sensors, the integrated radiation dose
 220 in the layer-3 mid-plane sensors, which are the most exposed in the SVD,
 221 is estimated to be 70 krad. The estimation is based on the correlation be-
 222 tween the SVD occupancy and the diamonds dose. The estimated dose in-
 223 cludes uncertainties of about 30% due to the unavailability of the appropri-
 224 ate trigger before December 2020. Assuming the dose/ n_{eq} fluence ratio of
 225 2.3×10^9 $n_{\text{eq}}/\text{cm}^2/\text{krad}$ from MC, 1-MeV equivalent neutron fluence is eval-
 226 uated to be about 1.6×10^{11} $n_{\text{eq}}/\text{cm}^2$ in the first two and a half years.

227 The effect of the integrated dose on the sensor leakage current is measured,
 228 and the results show a clear linear correlation as in the upper plot of Fig. 6.

229 The slopes for all the sensors are summarized in the lower plot of Fig. 6. They
230 are around 2–5 $\mu\text{A}/\text{cm}^2/\text{Mrad}$. The large variations can be explained by tem-
231 perature effects and the deviation of sensor-by-sensor dose from the average in
232 each layer used in the estimation. The slopes are in the same order of magni-
233 tude as previously measured in the BaBar experiment [8], 1 $\mu\text{A}/\text{cm}^2/\text{Mrad}$ at
234 20°C. While the leakage current is increasing, the impact on the strip noise is
235 suppressed by the short shaping time (50 ns) in APV25. It is expected to be
236 comparable to the strip-capacitive noise only after 10 Mrad irradiation and not
237 problematic for ten years where the integrated dose is estimated to be 2 Mrad.

238 The relation between the noise and the integrated dose is shown in Fig. 7.
239 The noise increase of 20–25% is observed in layer-3, but this does not affect the
240 performance of SVD. This noise increase is likely due to the radiation effects on
241 the sensor surface. Fixed oxide charges on sensor surface increase non-linearly,
242 enlarging inter-strip capacitance. The noise saturation is observed on the v/n-
243 side and also starts to be seen on the u/p-side. This behavior agrees with the
244 increase of fixed oxide charges.

245 The full depletion voltage of the sensor is also a key property that can be
246 affected by the radiation damage. It can be measured from the v/n-side strip
247 noise, which suddenly decreases at the full depletion voltage because the sensor
248 substrate is n-type and thus the v/n-side strips can be fully isolated at the full
249 depletion. From this measurement, reasonable full depletion voltages, which are
250 consistent with the values mentioned in Sec. 2, were confirmed, and so far no
251 change in full depletion voltage is observed in the first two and a half years of
252 operation, which is consistent with the expectation from low integrated neutron
253 fluence of $1.6 \times 10^{11} \text{ n}_{\text{eq}}/\text{cm}^2$.

254 5. Conclusions

255 SVD has been taking data in Belle II since March 2019 smoothly and reliably.
256 The detector performance is excellent and agrees with expectations. We are
257 ready to cope with the increased background in higher luminosity by rejecting

258 the off-time background hits using hit-time and operating in the three/six-mixed
259 acquisition mode. In the recent study, the efficiency loss in the three-samples
260 data is confirmed to be less than 0.1% for the trigger timing shift within ± 30 ns.
261 The observed first effects of radiation damage are also within expectation and
262 do not affect the detector performance.

263 **Acknowledgments**

264 This project has received funding from the European Union’s Horizon 2020
265 research and innovation programme under the Marie Skłodowska-Curie grant
266 agreements No 644294 and 822070. This work is supported by MEXT, WPI,
267 and JSPS (Japan); ARC (Australia); BMWFW (Austria); MSMT (Czechia);
268 CNRS/IN2P3 (France); AIDA-2020 (Germany); DAE and DST (India); INFN
269 (Italy); NRF-2016K1A3A7A09005605 and RSRI (Korea); and MNiSW (Poland).

270 **References**

- 271 [1] T. Abe, et al., Belle II Technical Design Report (2010). arXiv:1011.0352.
- 272 [2] Y. Ohnishi, et al., Accelerator design at SuperKEKB, Progress of Theoretical
273 and Experimental Physics 2013 (3), 03A011 (03 2013).
- 274 [3] S. Bacher, et al., Performance of the diamond-based beam-loss monitor sys-
275 tem of Belle II, Nucl. Instrum. Meth. A 997 (2021) 165157. arXiv:2102.04800.
- 276 [4] K. Adamczyk, et al., The belle ii silicon vertex detector assembly and me-
277 chanics, Nuclear Instruments and Methods in Physics Research Section
278 A: Accelerators, Spectrometers, Detectors and Associated Equipment 845
279 (2017) 38–42, proceedings of the Vienna Conference on Instrumentation
280 2016.
- 281 [5] M. J. French, et al., Design and results from the APV25, a deep sub-micron
282 CMOS front-end chip for the CMS tracker, Nuclear Instruments and Meth-
283 ods in Physics Research Section A: Accelerators, Spectrometers, Detectors
284 and Associated Equipment 466 (2001) 359–365.

- 285 [6] G. Rizzo, et al., The Belle II Silicon Vertex Detector: Perfor-
286 mance and Operational Experience in the First Year of Data Taking.
287 arXiv:<https://journals.jps.jp/doi/pdf/10.7566/JPSCP.34.010003>.
- 288 [7] R. L. Boucher, et al., Measurement of the cluster position resolution of the
289 Belle II Silicon Vertex Detector, these NIMA Conference Proceedings.
- 290 [8] B. Aubert, et al., The babar detector: Upgrades, operation and performance,
291 Nuclear Instruments and Methods in Physics Research Section A: Accelerators,
292 Spectrometers, Detectors and Associated Equipment 729 (2013) 615–
293 701.

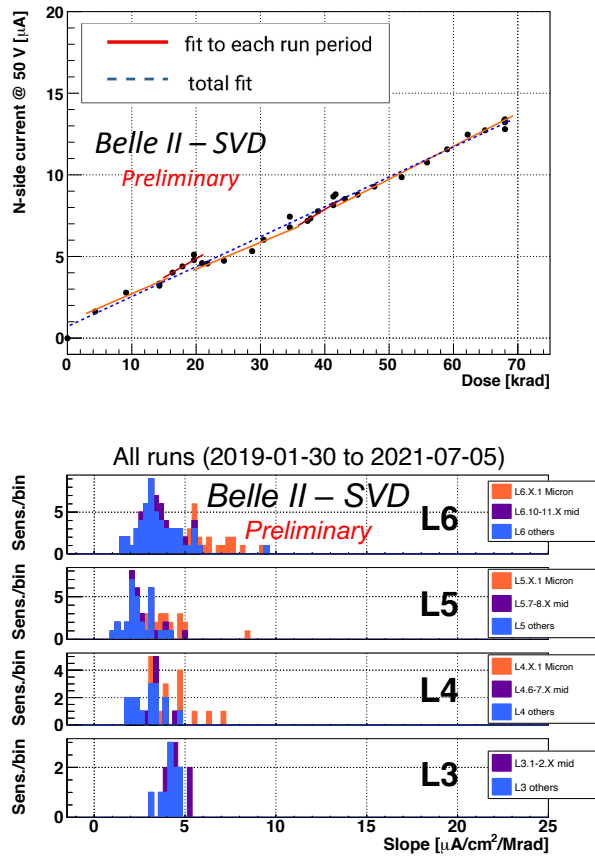


Figure 6: (upper) The effect of the integrated dose on the leakage current in the n/v-side of one layer-3 sensor. The slope is fitted for each run period (solid red line) and for all the runs (dashed blue line). Both fit results agree well with each other and are consistent with the linear increase. (lower) The fit results of all the sensors for all runs. The sensors are classified as trapezoidal sensors in the forward region, sensors around the midplane, and the others.

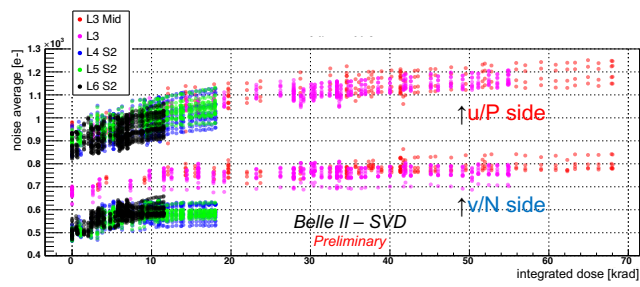


Figure 7: The effect of the integrated dose on the noise average in electron The clear increase is observed and saturated (or start to be saturated) for layer-3 sensors.